PCCP

The effect of weighted averages when determining speciation and structure-property relationships of europium(III) dipicolinate complexes

Journal:	*Physical Chemistry Chemical Physics*
Manuscript ID	CP-ART-02-2020-000989.R1
Article Type:	Paper
Date Submitted by the Author:	23-Apr-2020

Complete List of Authors:	Nawrocki, Patrick; University of Copenhagen, Nano-Science Center & Department of Chemistry Kofod, Nicolaj; University of Copenhagen, Nano-Science Center & Department of Chemistry Juelsholt, Mikkel; University of Copenhagen, Nano-Science Center & Department of Chemistry Sørensen, Thomas; University of Copenhagen, Nano-Science Center & Department of Chemistry Jensen, Kirsten Marie; Kobenhavns Universitet, Dept. of Chemistry;

ARTICLE

The effect of weighted averages when determining speciation and structure-property relationships of europium(III) dipicolinate complexes

Received 00th January 20xx,
Accepted 00th January 20xx

DOI: 10.1039/x0xx00000x

Patrick R. Nawrocki, Nicolaj Kofod, Mikkel Juelsholt, Kirsten M. Ø. Jensen and Thomas Just Sørensen*

Lanthanide(III) coordination chemistry in solution is inherently complicated by the lack of directional interactions and rapid ligand exchange. The latter can be eliminated in kinetically inert complexes, but remains a challenge in complexes between lanthanide(III) ions and smaller ligands. As multiple conformations and partial decomplexation is an issue even with multidentate ligands, it will influence the observed solution properties of complexes of smaller ligands common in the field of f-elements coordination chemistry such as acetylacetonates and dipicolinates. Here, europium(III) complexes with one, two and three dipicolinates were investigated in a series of 13 samples where the composition was varied from 0 to 3 equivalents of dipicolinate. While the results did show the formation of three distinct europium(III) dipicolinate complexes confirming the literature data on the system, clear discrepencies in speciation related properties were evident when comparing results from absorption and luminecence spectroscopy. It was concluded that the difference is due to the difference in time constant of the two experiments. Further it is shown that information obtained from luminescence arise from a weigthed average, and with discepencies between observed and actual concentration exceeding 25 % it is advised that weighted averages are taken into consideration when reporting on solution properties of lanthanide(III) complexes. From the resolved optical spectra of $[Eu(H_2O)_9]^{3+}$, $[Eu(DPA)(H_2O)_6]^{+}$, $[Eu(DPA)_2(H_2O)_3]^{-}$, and $[Eu(DPA)_3]^{3-}$ the excited energy levels and transition probabilities are determined, and it was concluded that both transition probability and ligand field effect on the microstates are different in all four species.

Introduction

The properties of the 4f-elements are unique and arise from the electron configuration [Xe]4f^x (x=0-14) typical of the trivalent lanthanides, where the distribution of 4f valence electrons does not extend beyond the xenon core.[1] The result is characteristic optical properties arising from intra configurational 4f-4f transitions,[2-6] and strong magnetic anisotropies.[7] This makes the lanthanides essential in diagnostic MRI,[8-13] high sensitivity bioassay,[14-16] clean energy production,[17, 18] and in various consumer products.[19, 20]

The challenge in lanthanide chemistry also arise from the shielded valence electrons. As orbital overlap is vanishing, lanthanide(III) ions do not participate in strong bonding. Therefore, the coordination geometry is defined by inter-ligand repulsion, and ligand exchange is rapid as the energy barrier for exchange significantly lower than the ambient energy. Thus, a dynamic equilibrium exists between several species in solutions of lanthanide complexes, even when the complexes are strongly thermodynamically favoured.[21-23]

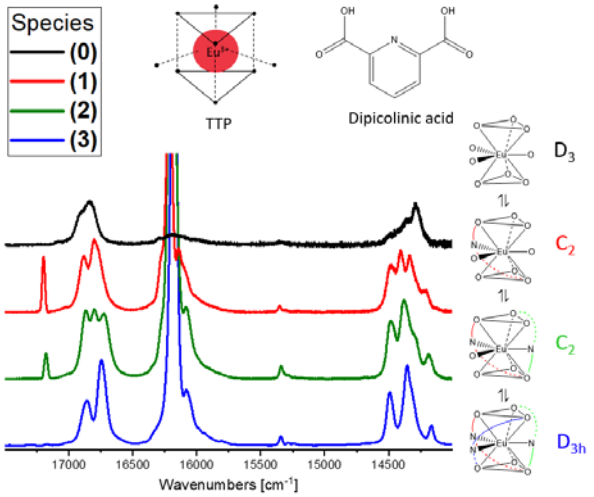

Figure 1. Top: The idealized tricapped trigonal prismatic (TTP) coordination geometry that the four investigated species: $[Eu(H_2O)_9]^{3+}$, $[Eu(DPA)(H_2O)_6]^{+}$, $[Eu(DPA)_2(H_2O)_3]^{-}$, and $[Eu(DPA)_3]^{3-}$ adopt in solution. Bottom: The resolved luminescence spectra of $Eu(H_2O)_9]^{3+}$, $[Eu(DPA)(H_2O)_6]^{+}$, $[Eu(DPA)_2(H_2O)_3]^{-}$, and $[Eu(DPA)_3]^{3-}$ normalised to show relative emission intensity and shown along the representative coordination polyhedral for the complex.

[a] Nano-Science Center & Department of Chemistry, University of Copenhagen, Universitetsparken 5, 2100 København Ø, Denmark.

† Footnotes relating to the title and/or authors should appear here.

Electronic Supplementary Information (ESI) available: Details on sample preparation; all optical spectra: absorption, luminescence emission, time-resolved emission decays and fits recorded; all results from speciation modelling: fits and parameters; and all results from total scattering experiments. See DOI: 10.1039/x0xx00000x

As a result, it can be hard to achieve a sample with a simple and known speciation in lanthanide chemistry in solution. This is particularly problematic in experiments where the time constant of the measurement is slow compared to the time constant of ligand exchange.[24] To investigate this issue we revisit europium(III) dipicolinate, a classic model system in lanthanide coordination chemistry.[25-34] Europium(III) exhibit strong luminescence in the visible part of the spectrum.[2, 29] In addition, the optical transitions are easier to interpret for europium(III) than e.g. terbium(III), because the ground state $^7F_0$ and principal emissive state $^5D_0$ are non-degenerate.[35] Further, the distribution of the microstates in the ^7F_J manifold and transition probabilities of the $^5D_0 \rightarrow {}^7F_J$ transition are strongly dependent on the coordination environment in the europium(III) complex.[36] The europium(III) centred luminescence is therefore rich in information, and can be used to probe local structure in crystals and the solution structure of europium(III) complexes.[16, 26, 37-41]

The early lanthanide(III) ions are typically nine coordinated with the tricapped trigonal prism (TTP) and the capped square anti-prism (CSAP) dominating their solution structures.[42-44] TTP is the ideal structure as the solution to the Thomson problem,[45] but restrictions imposed by the ligands can result in situations where CSAP symmetry is favourable. In this work, the structure of europium(III) aqua ion $[Eu(H_2O)_9]^{3+}$ and the coordinationally saturated tris-dipicolinate complex $[Eu(DPA)_3]^{3-}$ are both TTP with D_3 or D_{3h} symmetry.[27, 46, 47] The mono- and bis-dipicolinates are expected to have TTP coordination geometries of lower symmetries. The four complexes are $[Eu(H_2O)_9]^{3+}$ (**0**), $[Eu(DPA)(H_2O)_6]^{+}$ (**1**), $[Eu(DPA)_2(H_2O)_3]^{-}$ (**2**), and $[Eu(DPA)_3]^{3-}$ (**3**), the number indicating the number of dipicolinates in the inner coordination sphere.

Dipicolinate (DPA) is a common ligand for nine coordinate metal ions.[27, 31, 32, 48-55] The tridentate ligand forms highly symmetric, propeller-like coordination complexes, see Figure 1.[22, 26, 27, 32, 48, 51, 53, 56-67] Here, we were targeting the more elusive **(1)** and **(2)** complexes. **(1)** was included in the first reports,[27] but **(2)** was neglected until more detailed studies were undertaken.[48, 66] Here, the different symmetries of the four species—from aqua ion to tris-dipicolinate complex—were readily identified using optical spectroscopy. The different symmetries lead to four distinct emission spectra, see Figure 1.

If the speciation is to be determined from luminescence, either the quantum yield of the emitter must be the same in all species or the luminescence lifetime must be significantly shorter than the rate constant leading to interchange between species, see Figure 2.[68] Our detailed study revealed that emission data cannot be used to determine speciation in the europium(III) dipicolinate complexes in solution, as the millisecond lifetime of the emissive state is significantly slower than the ligand exchange.[21, 69-71] Thus, all emission data will report weighted averages, and speciation must be determined from absorption data.

We decided to explore the influence of the weighted average and determine the optical properties of the less known **(1)** and **(2)** complexes.

The problem of the weighted average is illustrated in Figure 2, where the speciation of two complexes with very different quantum yields—very different probabilities of spontaneous emission **A** (Einstein's constant for spontaneous emission)—are probed using either absorption or luminescence spectroscopy. In the former, the timescale of the experiment is too short to allow averaging due to ligand exchange to occur (fs vs µs). In contrast, europium(III) luminescence occurs on a timescale that is longer (ms vs µs), and as the structure changes the optical properties, ligand exchange actively perturbs the observed spectra. We were able to determine and eliminate the influence of the weighted average, by only using absorption data to determine speciation. We prepared 13 samples with varying europium(III) to dipicolinate ratios from 1:0 to 1:3. The aim was to create stable solutions of the three europium(III) dipicolinate complexes, not to determine the thermodynamic association constant that would require a fixed ionic strength across the series. Using data from the complete series, we were able to determine the speciation of each sample, which in turn provided the electronic energy levels and transition probabilities of each of the four species involved. The results show that both properties change significantly between the four europium(III) species. Finally, we are able to provide examples of when the weighted average has significant consequences for the observed spectra.

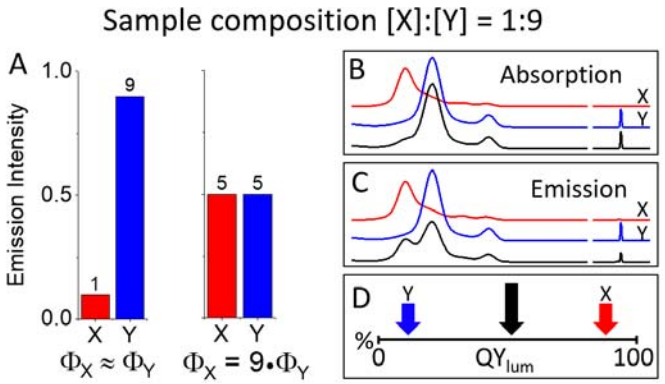

Figure 2. The effect of averages and weighted average on spectra and properties illustrated using a sample containing a 1 : 9 mixture of two lanthanide(III) complexes, X (red) and Y (blue) that undergo interconversion via rapid ligand exchange. A) the observed total emission intensity originating from the two species in the sample if the quantum yields of luminescence of X and Y are similar or very different. B) absorption spectrum (black) from the sample when X and Y are assigned distinct component spectra (X red, Y blue). C) emission spectrum (black) from the sample when X and Y are assigned distinct component spectra (X red, Y blue). D) The luminescence quantum yield (black arrow) observed in the sample. In C) and D the luminescence quantum yield of X is 9 times higher than that of Y.

Methods and Materials

99 % 2,6-Pyridinedicarboxylic acid and 99.9 % Eu_2O_3 were obtained from Sigma-Aldrich. Samples in deuterated water was

made from 35 wt% DCl and 40 wt% NaOD obtained from Sigma-Aldrich. All chemicals were used as received.
All measurements are carried out at ambient temperatures and within a day after mixing to prevent precipitation.

Sample preparation

13 samples were made in samples vials with a final volume of 5 ml and 20 mM europium(III) in each. A stock solution of europium(III) was made by dissolving 351.9 ± 2 mg in 20 ml 2 M HCl. In 13 different sample vials, DPA was weighed and transferred in order to obtain 0 to 60 mM DPA varying by 5 mM DPA for each sample and dissolved in 1 ml 2 M NaOH. 1 ml europium(III) stock solution is added to the DPA solution. pH is adjusted to 3 in all samples to dissolve precipitate. For pH < 2 flaky precipitate is seen while pH > 8 forms cloudy precipitate. The Eu.DPA complexes precipitate spontaneously after a few hours, typically.

Absorption spectroscopy

Absorption spectra were recorded on a Cary 300 Series UV-Vis Spectrophotometer. Spectra were recorded in the interval 300 - 600 nm with 1.1 s integration time, 0.2 nm data interval and 0.5 nm slit width. Additional spectra were recorded for the 580 nm transition peak. In the interval of 576.5 – 583.5 nm the integration time was set to 3 s, slits to 0.2 nm and a step size of 0.1 nm. A water sample was used for instrument calibration.

Luminescence spectroscopy

Steady state emission and excitation spectroscopy were measured on a PTI QuantaMaster 8075-22 Fluorimeter with a xenon arc lamp. Detector sensitivity was corrected with a factory provided correction file, and wavelength fluctuation corrected with a reference detector. Emission spectroscopy was recorded with λ_{ex} = 394 nm and 8 nm excitation slits, λ_{em} = 525 – 840 and 0.8 nm emission slits, data interval of 0.03 nm and 0.3 s integration time. The excitation spectra were recorded with similar setting, λ_{em} = 615 nm with 8 nm slit widths, λ_{ex} = 300 – 550 nm with 0.8 nm slits, data interval of 0.03 nm and 0.3 s integration time. The time-gated lifetimes were recorded at λ_{ex} = 394 nm with 8 nm slit widths, λ_{em} = 615 nm with 3 nm slits. The spectra are obtained in arbitrary intensity units. Time-gated intensity measurements to determined excited state lifetimes were also carried out on the PTI QuantaMaster 8075-22 Fluorimeter with λ_{ex} = 394 nm and detection at λ_{em} = 615 nm. The spectral band width was set to 8 nm for both excitation and emission. All decay traces were generally fitted to monoexponential decay functions using the built-in functions of Origin 2017, except for samples of Eu:DPA ratios of 1:2.50 and 1:2.75 where the monoexponential decay functions produced a poorer fit compared to a biexponential decay function.

Determining relative transition probability. In this study, the focus is on changes in the coordination environment, which influences the radiative rate constant of emission, k_{rad}. In lanthanide(III) complexes is k_{rad} predominately determined by the symmetry of the ligand field and relates directly to the Einstein coefficient of spontaneous emission, A.[72] Obtaining exact values of A is difficult. However, the relative changes across a series of samples with identical concentrations of the emitter can be obtained as this scenario allows several simplifications. The relative quantum yield of each sample can be obtained as shown in eq 1:

$$\Phi_{rel} = \frac{\int I^E(\lambda)d\lambda}{Abs};\ \Phi^{\lambda}_{rel} = \frac{I^E(\lambda)}{Abs} \qquad (1)$$

Where Φ_{rel} is the relative quantum yield, I^E is the integrated emission intensity and Abs is the absorption of the sample in the excitation window. The relative quantum yield can be determined for the emitting state or as a function of wavelength λ. The latter corrects the spectrum for changes in the absorption band, and thus removes changes due to variations in the number of photons absorbed by each europium(III) species in the sample.
The quantum yield relates to the rate constant of emission and the Einstein coefficient of spontaneous emission, A. The relative quantum yield can be used to determine the relative transition probability A_{rel} of a given line in the spectrum by normalizing by the observed rate constant of emission k_{obs}, as shown in eq. 2:

$$\Phi_{rel} = \frac{A_{rel}}{k_{obs}};\quad A^{\lambda}_{rel} = \frac{\Phi^{\lambda}_{rel}}{k_{obs}} \qquad (2)$$

Note that k_{obs} is the observed rate constant for the depopulation of all emitting (micro)states, and that k_{obs} is the inverse of the observed lifetime. This removes observed differences in emission intensity due to changes in nonradiative processes, primarily from the changes of O-H oscillators from the solvent. Thus, these calculations provide a quantity, $\mathbf{A}_{rel}$, that only dependents on the changes in transition probability i.e. changes in coordination geometry of the europium(III) ion. It should be noted that this quantity is a relative measure of transition probability, and a measure that it is directly proportional, but not equal to, the Einstein coefficient of spontaneous emission, see eq. 3.

$$A_{rel} \propto A = k_{Lm} = k_{Rad} = \frac{1}{\tau_0} \qquad (3)$$

Note that this treatment is valid for europium(III), as the multiplicity and ligand field splitting of the emitting state $^5D_0$ is invariant for all coordination geometries. The treatment assumes a single initial (micro)state but takes changes in multiplicity of the final state into account.

Determination of q. The number of coordinating solvent molecules (q) was determined using the modified Horrocks' equation shown in eq. 4.[22, 73, 74]

$$q = A\left(\left(\tau_{H_2O}\right)^{-1} - \left(\tau_{D_2O}\right)^{-1} - B\right) \qquad (4)$$

Here A is a lanthanide specific proportionality constant (0.6 ms pr. OH oscillator for Eu(III)), τ_{H_2O} and τ_{D_2O} are the observed lifetimes of the excited state in ms and B is a lanthanide specific correction factor for outer sphere solvent molecules (0.25 ms^{-1} for Eu(III)).

Speciation modelling. A modification of the EQUIL[75] algorithm, which has been implemented in the software DYNAFIT[76, 77] was used for modelling speciation of europium(III) across the samples. The algorithm applies to any given binding model or coupled equilibria. In the model the observed intensity of a given line in an absorption or emission spectra is given as a sum of the intensity of each species in solution, eq. 5. By using molar absorptivity, rate of emission, and excited state lifetimes, an intrinsic model can be used, as all values is a function of molar fraction of the involved species:

$$I_{obs} = \sum_{i=1}^{n_x} I_i \cdot c_i / \sum_{i=1}^{n_x} c_i \qquad (5)$$

Where I_{obs} is the observed spectral intensity, n_x is the number of possible species present in solution, I_i is the spectral intensity of a given species and c_i is the concentration of a given species at equilibrium. The binding constants are contained in the equilibrium concentrations. Binding constants and the intrinsic intensities were treated as adjustable parameters. The observed intensities were fitted using a nonlinear least-squares regression of equation 1 and the hybrid trust-region algorithm.[78] All signals were fitted globally. For binding constants nonsymmetrical 95% confidence intervals were estimated using the profile-T method by Bates and Watts.[79] In this study, the binding constants were determined from absorption data only, as the long excited state lifetime of Eu(III) introduces dynamic effects from ligand exchange in the emission data. The determined model describes the general features of the full data set, but some features of the emission data are not contained within the model. This is described in more detail below. From the determined binding constants, the speciation in solution as a function of dipicolinate concentration was simulated. All data, fits, confidence interval profiles, and individual speciation traces are available in the SI.

The calculated binding constant were used as input values to simulate a speciation model, see Figure S38. In the model the species responses are plotted against ligand concentration. By normalizing the response of each curve we obtain the molar fractions c_i of the species involved. The molar fractions are collected in Table S2. The first sample of the experimental series contain no DPA and the spectra of this sample will consist of $[Eu(H_2O)_9]^{3+}$ exclusively. Similarly, the spectral shape of $[Eu(DPA)_3]^{3-}$ can be obtained directly from the sample with three equivalents of DPA. In this sample, $[Eu(DPA)_3]^{3-}$ makes up 99.8 % of the Eu(III) species as predicted by the speciation model. From the spectra of $[Eu(H_2O)_9]^{3+}$ and $[Eu(DPA)_3]^{3-}$ the spectral shapes of **(1)** and **(2)** can be derived. A proper representation of the spectra can be obtained by subtracting the spectral shape of **(0)** or **(3)** species of Eu(III) from the spectra obtained from other samples in the series. After subtraction and subsequently rescaling the spectra the deconvoluted spectra can are obtained. The four deconvoluted spectra are shown in Figure 6.

Determination of Excited State Energies

The electronic energy levels were determined from the deconvoluted spectra in absorption and emission spectroscopy. The energy levels of absorption were chosen as the point of intersection between the backgrounds standard deviation, 1σ, with the tangent line of the fitted peak center *minus* the fwhm. In the emission peaks the tangent line of the peak center *plus* the fwhm was used instead. The determined excited state energy levels are reported in Table S3 and S4.

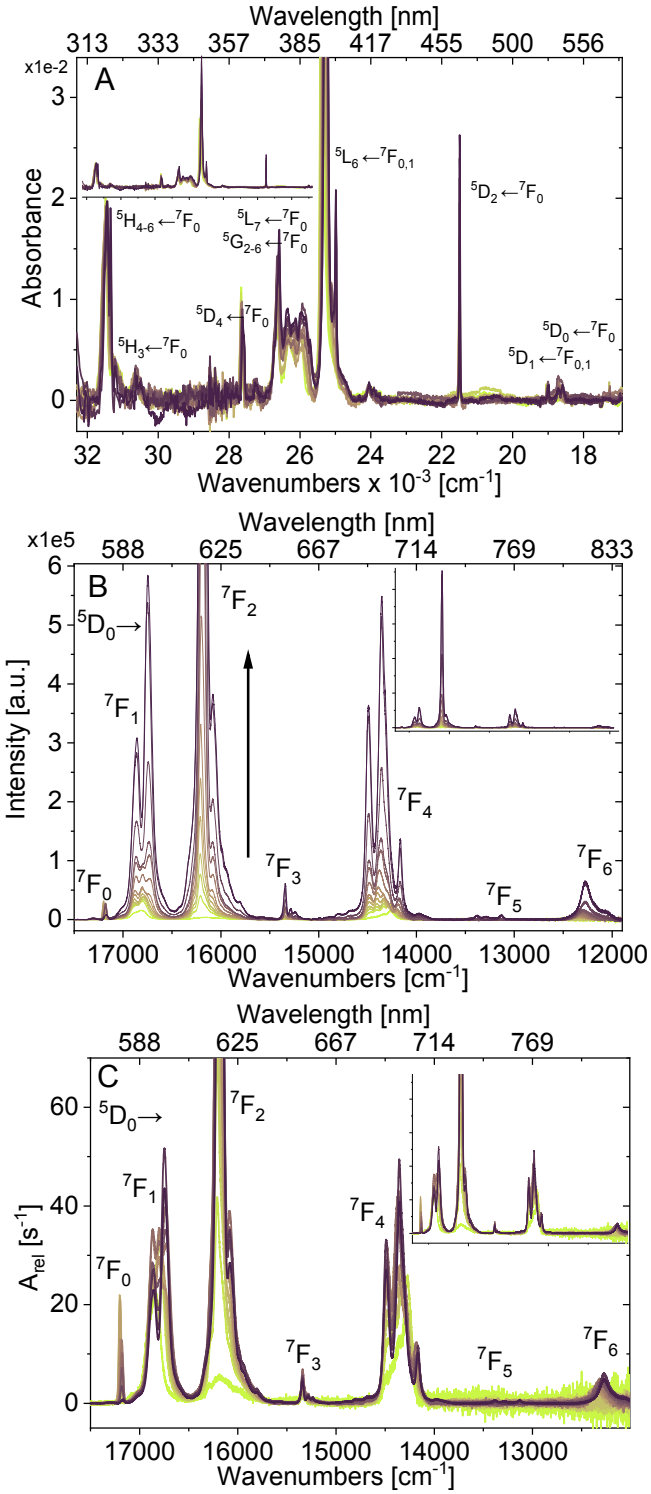

Figure 3. Optical spectra recorded from the thirteen aqueous solutions with a constant europium(III) concentration of 0.02 M and a constant concentration of dipicolinic acid from 0 to 0.06 M (black). A, absorption spectra recorded in a 1 cm cuvette and shown with an insert that includes the full peak at 392 nm. B, steady state

luminescence emission spectrum following excitation at 394 nm with 8 nm excitation slit and 0.8 nm emission slits, the insert shows the full spectrum. C, steady state luminescence emission spectrum divided by the fraction of absorbed light and the observed rate constant of luminescence.

X-ray Total Scattering

X-ray Total scattering data were obtained at Argonne National Laboratory's Advanced Photon Source beamline 11-ID-B using a wavelength of 0.2113 Å. The detector distance was kept at 125 mm. All scattering data were obtained at room temperature.

The X-ray total scattering data were treated by first integrating 2D-images in Fit2D.[80] Further treatment (normalization and Fourier transformation) was done using PDFgetX3[81] to obtain Pair Distribution Functions (PDFs).

Results and Discussion

The coordination of dipicolinic acid (DPA) to europium(III) ions in aqueous media was studied by preparing a series of 13 samples with constant europium(III) concentration of 0.02 M and a concentration of dipicolinic acid from 0 (yellow) to 0.06 M (brown). The ionic strength and pH of the samples were optimised to prevent precipitation. Note that pH and ionic strength are not constant throughout the series, however the pH of the samples were near 3. The focus is the structure of the complexes, and relative binding constants are used to describe speciation in the samples.

Figure 3 shows the optical spectra recorded from all samples. It is evident that the addition of DPA changes the spectra. It has been established that small changes in the coordination sphere of europium(III) ions can be seen as changes in band shapes and intensities in the europium(III) emission spectra.[1-4, 28, 36, 66, 82-86] And as all spectra are recorded using direct excitation of the europium(III) centre, all spectral changes are directly linked to changes europium(III) speciation.

Prior to analysing the spectra, it is important to note three things: *i*) all spectra are only addressing europium(III) centred transitions, *ii*) the concentration of europium(III) is constant in all samples, and *iii*) the emission spectra y-axis is directly proportional to transition probability because the emission spectra are corrected for absorption at the point of excitation and the rate of non-radiative deactivation.

Considering the spectra in Figure 3, it is evident that the absorption spectra are directly comparable. It is also evident that the process of going from emission intensity **I** to the relative transition probability $\mathbf{A}_{rel}$ is essential, as the rate of non-radiative deactivation—the degree of quenching—is very different in the four species.

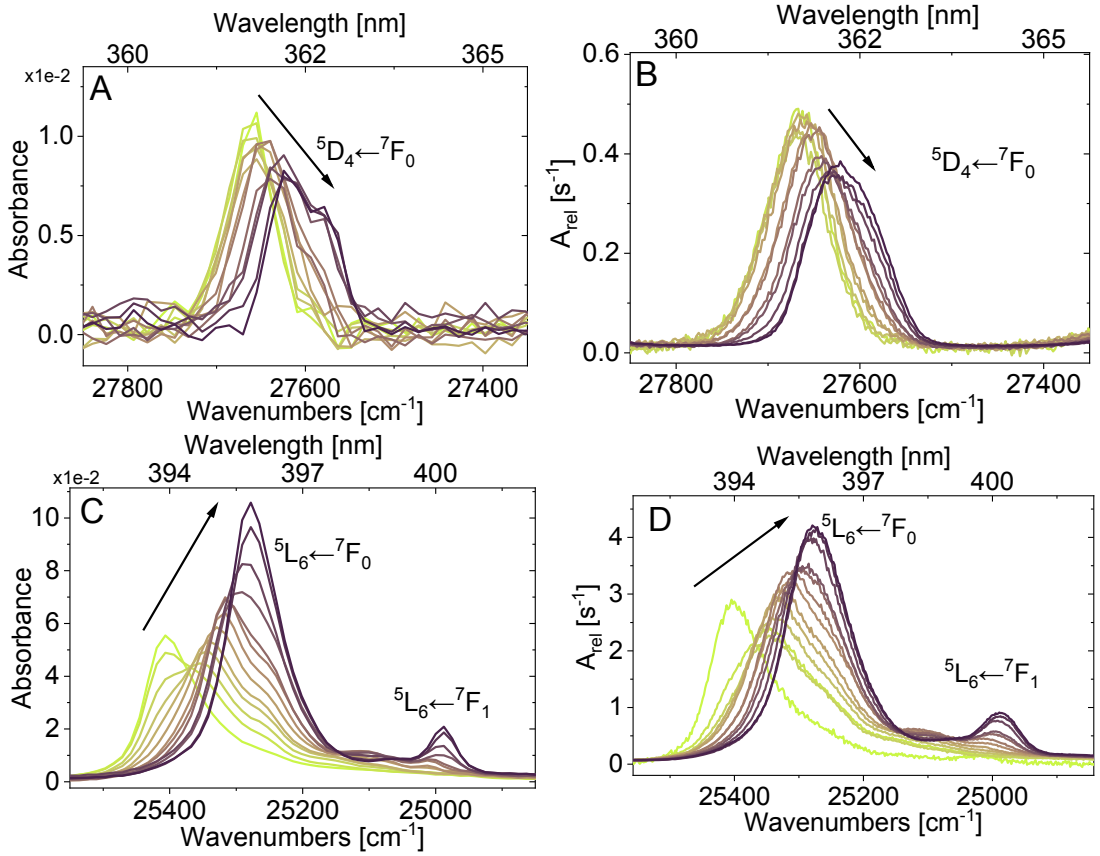

Figure 4. Optical spectra recorded from the thirteen aqueous solutions with a constant europium(III) concentration of 0.02 M and a concentration of dipicolinic acid from 0 to 0.06 M (black). A and C, absorption spectra recorded in a 1 cm cuvette. B and D, steady-state luminescence excitation spectra following 615 nm emission using 0.8 nm excitation slits and 8 nm emission slits, the spectra are normalised by the area of the ^5H_J band.

Speciation

The four species that are present in the 13 samples are $[Eu(H_2O)_9]^{3+}$ (**0**), $[Eu(DPA)(H_2O)_6]^{+}$ (**1**), $[Eu(DPA)_2(H_2O)_3]^{-}$ (**2**), and $[Eu(DPA)_3]^{3-}$ (**3**). The four species differ in symmetry and number of coordinated water molecules, yet are all expected to be in a tricapped trigonal prism coordination geometry as shown in Figure 1. As the luminescence lifetime changes due to both changes in transition probability and amount of quenching, the quantum yields are very different and the amount of the component spectrum of a species observed in the emission spectrum will be different from actual concentration of the species. This is illustrated in Figure 2 where the quantum yields of two systems differ significantly.

Considering all the data given in the ESI it is readily recognised that the data from luminescence spectra arise from a weighted average. The component spectrum of one species is overrepresented due to a higher emission quantum yield and a ligand exchange faster than the observed rate of luminescence.[68] The data in Figure 4 was chosen to illustrate this observation.

The effect of the weighted average can be seen by comparing absorption spectra to excitation spectra. The $^7F_0 \rightarrow {}^5D_4$ transition (Figure 4A and 4B) have a distinct band for all four species, with a continuously decreasing transition probability and a centre wavelength shifting to lower energy. Although this progression is clearly documented in the absorption spectrum, the excitation spectrum does not contain the same amount of information. This is even more clear in the $^7F_0 \rightarrow {}^5L_6$ transition (Figure 4C and 4D), where the bands corresponding to the two high symmetry species, **(0)** and **(3)**, are strongly underrepresented in the excitation spectrum. This to the point where the band of the europium(III) aqua ion near instantly become undiscernible as soon as dipicolinate is introduced to the solution. The absorption spectra of the $^7F_0 \rightarrow {}^5L_6$ transition in Figure 4C includes three isosbestic points, proving that we have four species in solution. Very little of this information is available in the excitation spectra in Figure 4C, although the change in speciation can be followed. The issue is then if the change in the concentration of the individual species is accurately reflected by the luminescence data.

As we assume that the luminescence data is a weighted average, the speciation across the 13 samples was determined using absorption data only. The isotherms used are included in the electronic supplementary information, and the resulting speciation is shown in Figure 5A. To determine how large an error the weighted average introduces when speciation is determined using luminescence data, a plot of the speciation determined from emission data is imposed on the actual speciation in Figure 5B. It is clear that significant errors (>10 %) is introduced in almost all samples if luminescence data is taken to represent concentrations of a given species. The ligand exchange is too fast and the difference in transition probability is too large for luminescence to be representative of concentration. Further, the properties determined from a sample will not directly correlate to the amount of species present. Figure 5B shows that the luminescence data report the presence of 8% **(2)** in the final sample of the titration series when in fact only 0.2% of **(2)** is present.

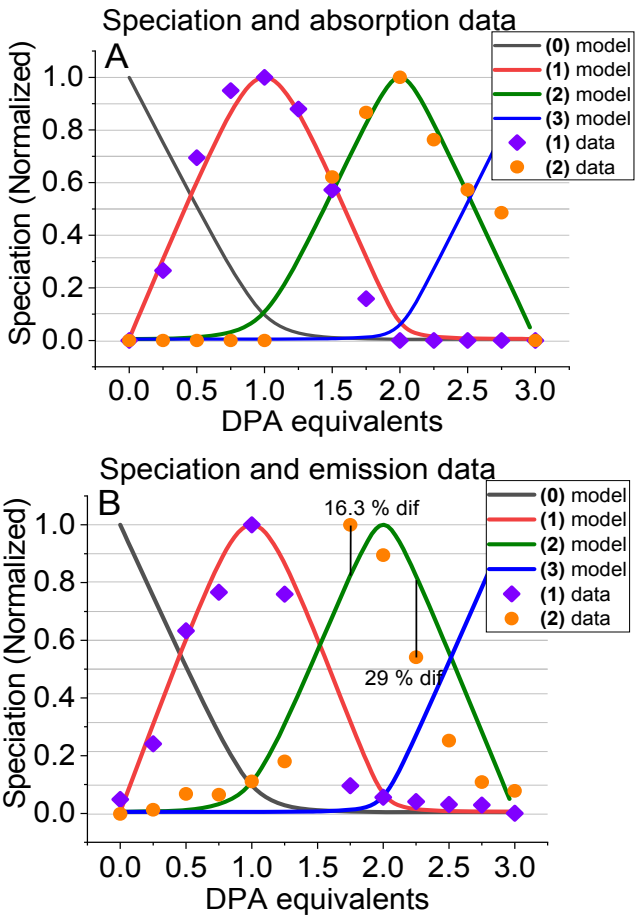

Figure 5. Normalized models of speciation plotted against ligand concentrations in equivalents to Eu(III). Integrated spectral intensities are superimposed onto the graph to reflect the experimental change in response as [DPA] is varied. The models describe the molar fraction of the four species of $[Eu(H_2O)_9]^{3+}$ (**0**, black), $[Eu(DPA)(H_2O)_6]^{+}$ (**1**, red), $[Eu(DPA)_2(H_2O)_3]^{-}$ (**2**, green), and $[Eu(DPA)_3]^{3-}$ (**3**, blue). The data points reflect the area of the symmetry dependant transitions between the $^5D_0$ and $^7F_0$ states originating from the transition band of $[Eu(DPA)(H_2O)_6]^{+}$ (purple) or $[Eu(DPA)_2(H_2O)_3]^{-}$ (orange).

Thus all luminescent properties reported for a 1:3 mixture of europium(III) and dipicolinate in water, assumed to arise exclusively from compound **(3)**, may include a contributions as large as 10 % from **(2)**.

It should be emphasized that the weighted average is an issue of differences in the magnitude of experimental response between different species, as illustrated in Figure 2. In the case of NMR the peak magnitude will not vary with the species but only affect the chemical shift, see Figure S44.

As the speciation is known, the contribution of each species in all spectra are known, and we are able to resolve the component absorption, excitation and emission spectrum of each of the europium(III) species. The spectra of **(0)**, **(1)**, **(2)**, and **(3)** are shown in Figure 6, and are in good agreement with those previously published.[27, 28, 66]. These spectra allow a detailed analysis of the relationship between solution structure and

electronic energy levels and photophysical properties as discussed further below.

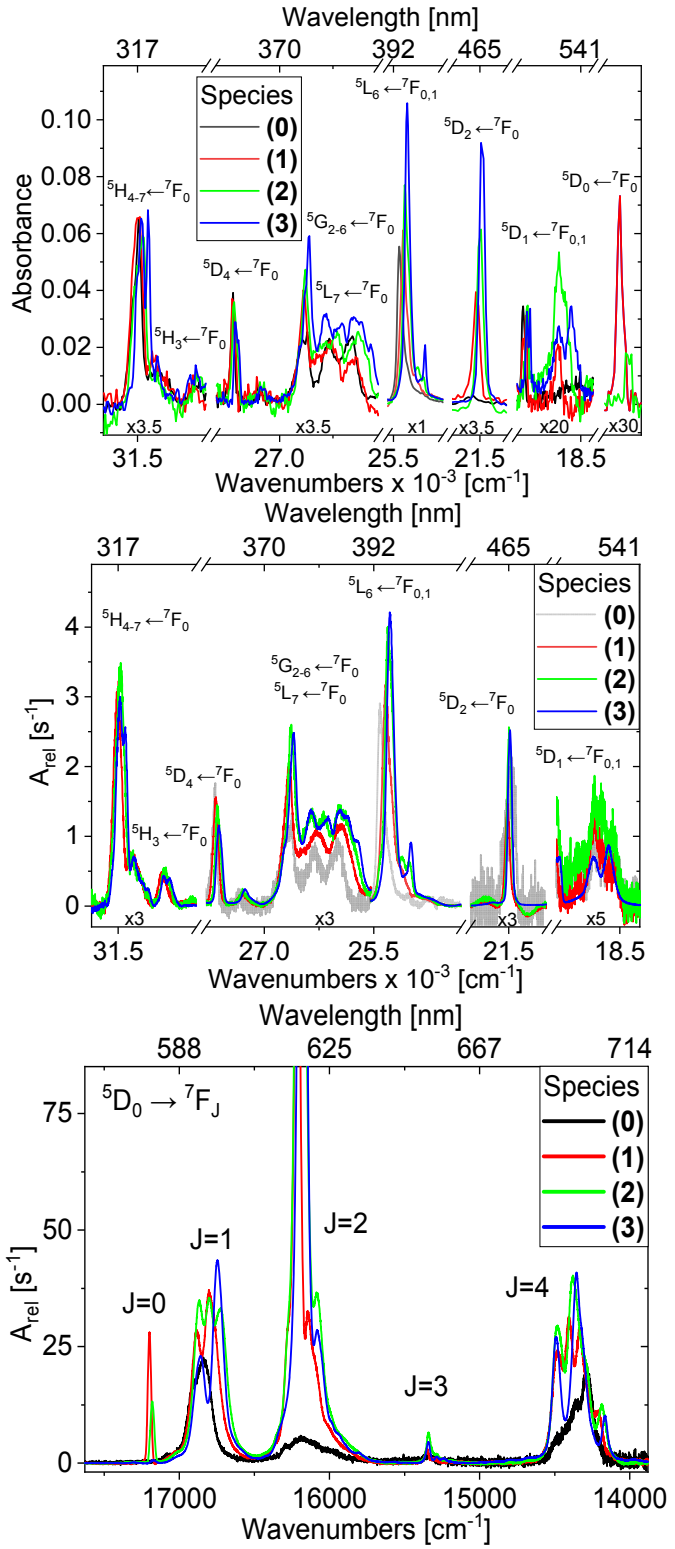

Figure 6. Deconvoluted absorption (top), excitation (center) and emission (bottom) spectra of the four europium species $[Eu(H_2O)_9]^{3+}$ (**0**, black), $[Eu(DPA)(H_2O)_6]^{+}$ (**1**, red), $[Eu(DPA)_2(H_2O)_3]^{-}$ (**2**, green), and $[Eu(DPA)_3]^{3-}$ (**3**, blue). Each spectrum represents the actual spectral response of a species without contributions from others europium(III) species.

Structural characterisation

To further support the assigned solution structure we obtained X-ray total scattering data from the thirteen solutions.[87-89] However, the low concentration of the species in the solutions challenges PDF analysis of the data. While formation of the complexes could be confirmed, see Figure S46, we were not able to determine the solution structure from PDF. Better data quality could be obtained with higher europium(III) and dipicolinate concentrations, however this would favour precipitation in the solutions. Thus, we are limited to the indirect information carried by the optical spectra.[35, 66, 90-92]

Photophysical properties of europium(III) dipicolinate complexes

Figure 6 shows the optical spectra of **(0)**, **(1)**, **(2)**, and **(3)**. These reveal the electronic energy levels in the europium(III), and in several cases the splitting of the microstates within each electronic energy level. These reflect the ligand field of the complex and will differ between the species.[35-37, 93-97]

All the spectra in Figure 6 are recorded from samples arising from a single stock solution of europium(III). Thus, the europium(III) concentration is constant across all spectra. Further, all spectra are corrected and recorded using identical settings. Therefore, we can compare the transition probabilities directly in the absorption spectra and calculate both relative quantum yield Φ_{rel} and relative transition probability $\mathbf{A}_{rel}$ from the emission spectra, see above. We decided to plot the spectra as $\mathbf{A}_{rel}(\lambda)$ as this allows the relative transition probability of each line in the spectrum to be compared directly, if they are resolved.

As a model system, europium(III) dipicolinate complexes have been studied extensively.[26, 27, 48, 49, 98] Werts *et al* treated the photophysics of **(0)**, **(1)**, and **(3)** in 2002. Rather than comparing relative transition probabilities, they compared the integrated intensities of each band in spectra where the total area was normalised to unity. This is called the branching ratio. In Table 1 we have plotted the relative transition probabilities within each band. Note that the transition probability is per line. Unless the individual lines are resolved, it cannot be discerned if a high transition probability determined over a band is due to a single strong line or a set of several intermediate lines. This is an important fact to note when considering lanthanide photophysics, as almost all observed bands consist of several transitions between distinct electronic states in the same manifold thus cannot be treated as a single electronic transition with a vibronic envelope.

Europium(III) is different as the principal emissive state $^5D_0$ is a single electronic energy level. $^5D_0$ consist of a single microstate and is traditionally described as being non-degenerate. The same is true for the ground state $^7F_0$, and the transition between these two microstates is a single line. In the dipicolinate complexes of europium(III) the transitions from $^5D_0$ to the three microstates of state $^7F_1$ are also resolved, see Figure 6. In **(1)** and **(3)** two lines with a ratio between the transition probability of

1:2 are observed. The three transitions are thus equally probable, and two out of three microstates are degenerate. In **(2)** all three lines are observed, and it can be seen that they are of equal probability. The number of microstates in the other bands are much higher than the number of lines that are resolved in the spectra, and does not allow for a similar analysis. If we assume that the transition probability per line is the same—although a highly improbable assumption—we can calculate the average transition probability see Table S6. As expected, even when taking the number of transitions in each band into account, the transitions from $^5D_0$ to the microstates in the $^7F_1$ and $^7F_2$ band remain much more intense than the other lines in the spectra. More surprising, the analysis reveals that the $^5D_0 \rightarrow {}^7F_0$ transition, which is designated as highly forbidden,[35, 91] can have the same transition probability as the individual lines in the $^5D_0 \rightarrow {}^7F_4$ band.

In addition to allowing complexes with very different quantum yield to be shown in the same graph, plotting $\mathbf{A}_{rel}(\lambda)$ allows the effect of the ligand field to be discerned directly. Cursory inspection of Figure 6 reveals that the overall transition probability is lower for the aqua ion than for the dipicolinate complexes, and that all the dipicolinate complexes have similar overall transition probability. Calculating the integrated $\mathbf{A}_{rel}$ for each species (Table 1) show there is a difference between the overall transition probability $\mathbf{A}_{rel}$ between complexes. While the all oxygen donor atom ligand field of the aqua ion has the highest symmetry and the lowest $\mathbf{A}_{rel}$, the differences between the complexes cannot be ascribed directly to symmetry. **(2)** has the highest $\mathbf{A}_{rel}$, but $\mathbf{A}_{rel}$ for **(3)** is higher than that of **(1)**. Inspection of the data summarised in Table 1 shows that the $^5D_0 \rightarrow {}^7F_0$ transition depends on symmetry but for the total $\mathbf{A}_{rel}$ this does not appear to be the case.

Table 1. Integrated emission intensity shown in terms of A_{rel} for each of the $^5D_0 \rightarrow {}^7F_J$ transitions for the four europium(III) species: $[Eu(H_2O)_9]^{3+}$ (**0**), $[Eu(DPA)(H_2O)_6]^+$ (**1**), $[Eu(DPA)_2(H_2O)_3]^-$ (**2**), and $[Eu(DPA)_3]^{3-}$ (**3**). The branching ratios shown in parenthesis indicate each bands relative contribution to the spectrum.

Band / degeneracy	(0)	(1)	(2)	(3)
$A_{rel}(^5D_0 \rightarrow {}^7F_0) / 1$	-	0.71 (0.03)	0.40 (0.02)	0.02 (0.00)
$A_{rel}(^5D_0 \rightarrow {}^7F_1) / 3$	3.74 (0.46)	6.45 (0.25)	8.11 (0.20)	6.30 (0.17)
$A_{rel}(^5D_0 \rightarrow {}^7F_2) / 5$	1.26 (0.15)	11.59 (0.44)	22.13 (0.54)	22.58 (0.62)
$A_{rel}(^5D_0 \rightarrow {}^7F_3) / 7$	-	0.11 (0.00)	0.35 (0.01)	0.24 (0.01)
$A_{rel}(^5D_0 \rightarrow {}^7F_4) / 9$	3.21 (0.39)	6.78 (0.26)	8.23 (0.20)	6.36 (0.17)
$A_{rel}(^5D_0 \rightarrow {}^7F_5) / 11$	-	-	-	0.09 (0.00)
$A_{rel}(^5D_0 \rightarrow {}^7F_6) / 13$	-	0.61 (0.02)	0.75 (0.03)	0.85 (0.02)
A_{rel} (Total)	8.21	26.3	40.0	36.4

The analysis of overall transition probability and branching ratio has also been performed by Werts et al and Bünzli et al,[28, 99] and our result for branching ratio and relative transition probabilities are within 5% of the literature values. We do not compare the data for the aqua ions, as small differences in sample composition drastically changes the observed properties.[68]

In the literature, the primary methodology used to describe the photophysics of europium(III) dipicolinates has been based on Judd-Ofelt theory.[4, 82] Parametrization using Judd-Ofelt was later optimized using transition probabilities normalized by assuming a constant transition probability of the $^5D_0 \rightarrow {}^7F_1$ band,[28, 81] however this treatment are only valid if the transition probability of the $^5D_0 \rightarrow {}^7F_1$ band is invariant with respect to the environment.

Our approach uses fundamental molecular photophysics, where the theoretical description of 'forbidden' electronic transitions remains an unsolved problem.[84, 100-102] Although there is no doubt that the transitions in the $^5D_0 \rightarrow {}^7F_1$ band have a significant contribution from a magnetic transition dipole,[103, 104] we have not found a convincing argument as to how this corresponds to a transition probability that is independent of electronic structure. Note that without heavy use of perturbation theory, quantum chemistry would predict that none of the transitions in europium(III) would be possible. More importantly, we have not been able to find experimental data in the literature that proves that the transition probability of the $^5D_0 \rightarrow {}^7F_1$ band is constant. As experimentalist we can only conclude that our data show that the transition probability of the $^5D_0 \rightarrow {}^7F_1$ band vary by a factor of two, and that is a similar order of magnitude as the variation in the $^5D_0 \rightarrow {}^7F_3$ and the $^5D_0 \rightarrow {}^7F_4$ bands.

Leaving aside the nature of the transitions, we turn to the experimental determination of transition probabilities. Using the Strickler-Berg formalism the transition probability can be reported as the oscillator strength *f*, [84, 105-107] or given as the dipole strength D.[27, 99] Note that this treatment completely ignores the number of m_J levels in each band and the effect of the refractive index when converting radiative lifetimes to oscillator strengths as done for the $^5D_0 \rightarrow {}^7F_0$ transition in Table 2. The other transitions observed in the absorption spectrum are not emissive, as the non-radiative deactivation is fast and—disregarding thermal population of $^5D_1$—the Kasha-Vavilov rule holds for europium(III).

Table 2. Spontaneous emission probability, A, calculated from the emission band barycentre and the integrated absorption band for species $[Eu(DPA)(H_2O)_6]^+$ (**1**) and $[Eu(DPA)_2(H_2O)_3]^-$ (**2**).

$^5D_0 \leftrightarrow {}^7F_0$	(1)	(2)
Emission energy [cm^{-1}]	17198.90	17179.90
ε, integrated [$cm^{-1}M^{-1}$]	1.4595	0.3795
A [s^{-1}]	12.43	3.226

The bands in the absorption and emission spectra were resolved, and the relevant edge of each band was used to determine the electronic energy levels in **(0)**, **(1)**, **(2)**, and **(3)**, see Tables S3 and S4. For the bands in the absorption spectrum the oscillator strength *f* and the dipole strength D was computed and compared to the values reported by Binnemans.[27] Table 3 shows the photophysical properties determined for **(0)**, **(1)**, **(2)**, and **(3)**. The dipole strength is included for comparison to literature values. We prefer to use the oscillator strength, as it can be compared to the oscillator strengths *f* known from molecular photophysics. Most intraconfigurational *f-f* transitions observed in lanthanide(III)

Table 3. Photophysical properties: integrated absorption, oscillator strength, and dipole strength of each transition observed in the absorption spectrum of $[Eu(H_2O)_9]^{3+}$ (**0**), $[Eu(DPA)(H_2O)_6]^{+}$ (**1**), $[Eu(DPA)_2(H_2O)_3]^{-}$ (**2**), and $[Eu(DPA)_3]^{3-}$ (**3**). Induced Electric Dipole selection rules (IED)

Absorption	Integrated ε				Experimental *f* x 10^6				Experimental D x 10^6				Reported[27] D x 10^6							
	(0)	(1)	(2)	(3)	(0)	(1)	(2)	(3)	(0)	(1)	(2)	(3)	(0)	(1)	(2)	(3)	ΔS	ΔL	ΔJ	Type
$^5H_{4\text{-}7}\leftarrow{}^7F_0$	214.7	231.7	240.1	231.7	9.43	10.1	10.5	10.1	63.7	68.7	71.2	68.8	--	--	--	--	1	2	--	forbidden
$^5H_3\leftarrow{}^7F_0$	20.0	24.0	24.3	43.1	0.88	1.05	1.07	1.89	6.1	7.3	7.4	13.1	--	--	--	--	1	2	3	forbidden
$^5D_4\leftarrow{}^7F_0$	29.5	34.1	41.6	31.0	1.30	1.50	1.83	1.36	10.0	11.5	14.1	10.5	17	17	--	16	1	1	4	forbidden
$^5G_J,{}^5L_7\leftarrow{}^7F_0$	204.3	268.0	332.0	370.2	8.97	11.7	14.5	16.2	72.3	94.8	117.	131.	85	84	--	132	1	1,5	-,7	forbidden
$^5L_6\leftarrow{}^7F_{0,1}$	385.8	562.7	620.1	706.4	16.9	24.7	27.2	31.0	142.	207.	229.	261.	213	234	--	353	1	1	6,5	IED
$^5D_2\leftarrow{}^7F_0$	1.0	16.3	28.2	36.2	0.05	0.72	1.24	1.59	0.5	7.1	12.2	15.7	3	11	--	23	1	1	2	forbidden
$^5D_1\leftarrow{}^7F_0$	3.1	3.5	3.3	3.2	0.13	0.15	0.14	0.14	1.5	1.7	1.6	1.6	2	2	--	2	1	1	1	forbidden
$^5D_1\leftarrow{}^7F_1$	--	3.1	14.1	10.4	--	0.13	0.61	0.45	--	1.5	7.0	5.2	2	10	--	21	1	1	0	forbidden
$^5D_0\leftarrow{}^7F_0$	--	1.465	0.385	--	--	0.06	0.01	--	--	0.8	0.2	--	--	--	--	--	1	1	0	forbidden

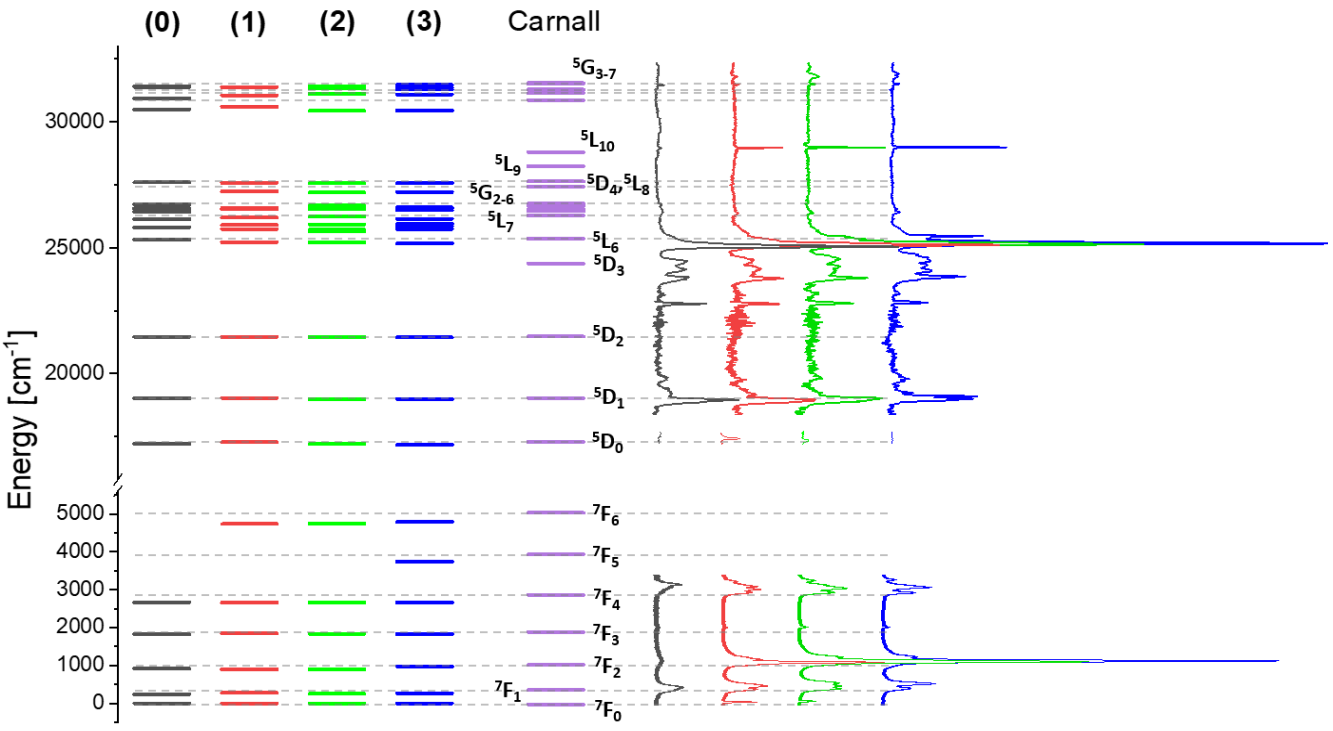

Figure 7. Energy level diagram for europium(III) in the four species **(0)**, **(1)**, **(2)** and **(3)** illustrated against the energy levels calculated by Carnall et al.[1] The emission (bottom) and absorption spectra (top) of the four species are shown for reference.

ions have *f* in the order of 10^{-6} to 10^{-7}, which is comparable to allowed singlet-triplet transitions in organic chromophores.[108, 109] One of the exceptions is the $^5L_6\leftarrow{}^7F_{0,1}$ transition, which is ten times more probable. A fact that is reflected by the relatively intense absorption band at 392 nm in all europium(III) absorption spectra.

While the transition probabilities determined in the absorption spectrum had to be determined for each band, we are able to consider the microstates when describing the electronic energy levels. And where we are able to resolve the microstates from the spectra we can probe the ligand field in the complexes. First we consider Figure 7 and Table 4, where the electronic energy levels of $[Eu(H_2O)_9]^{3+}$ **(0)**, $[Eu(DPA)(H_2O)_6]^{+}$ **(1)**, $[Eu(DPA)_2(H_2O)_3]^{-}$ **(2)**, and $[Eu(DPA)_3]^{3-}$ **(3)** are shown and tabulated. As we have the pure component spectra, we are able to resolve electronic energy levels of the four species, and compare them to the

Table 4. Electronic energy levels of europium(III) determined for the four dipicolinate species $[Eu(H_2O)_9]^{3+}$ (**0**), $[Eu(DPA)(H_2O)_6]^{+}$ (**1**), $[Eu(DPA)_2(H_2O)_3]^{-}$ (**2**), and $[Eu(DPA)_3]^{3-}$ (**3**). The determined energy levels are listed against the calculated and observed values of Carnall of aqueous europium(III).[1]

Term	**(0)**	**(1)**	**(2)**	**(3)**	**(0)**[1] Carnall	Calculated Carnall
$^7F_0$ [a]	0	0	0	0	0	-31
$^7F_1$ [a]	241	277	256	266	360	350
$^7F_2$ [a]	920	899	899	978	1020	1018
$^7F_3$ [a]	1828	1849	1837	1830	1887	1880
$^7F_4$ [a]	2668	2660	2664	2664	2865	2866
$^7F_5$ [a]	--	--	--	3742	3908	3927
$^7F_6$ [a]	--	4735	4746	4790	4980	5029
$^5D_0$ [b]	17211	17272	17206	17171	17277	17286
$^5D_1$ [b]	19019	19032	18982	18985	19028	19026
$^5D_2$ [b]	21495	21487	21476	21460	21519	21499
$^5D_3$ [b]	--	--	--	--	24408	24389
$^5L_6$ [b]	25338	25237	25230	25193	25400	25375
$^5G_2$ [b, c]	25830	26540	26685	26609	26300	26296
$^5G_3$ [b, c]	26147	26590	26552	26596	--	26469
$^5G_4$ [b, c]	26435	26211	26252	26510	--	26535
$^5G_5$ [b, c]	26536	25916	25946	26167	26620	26672
$^5G_6$ [b, c]	26581	25920	25729	25963	--	26733
$^5L_7$ [b, c]	26738	25765	25663	25880	26700	26762
? [b, c]	--	--	--	25757	--	--
$^5L_8$ [b]	--	27250	27201	27228	--	27435
$^5D_4$ [b]	27602	27594	27575	27582	27670	27641
$^5L_9$	--	--	--	--	--	28244
$^5L_{10}$	--	--	--	--	--	28813
$^5H_3$ [b]	30501	30606	30436	30457	--	30863
$^5H_7$ [b, c]	30937	31380	31405	31468	--	31145
$^5H_4$ [b, c]	31386	31383	31330	31358	31250	31281
$^5H_5$ [b, c]	31411	31053	31120	31291	--	31512
$^5H_6$ [b, c]	--	--	--	31091	31520	31539

[a] Determined from luminescence spectroscopy at the blue edge of the emission band. [b] Determined from absorption spectroscopy at the red edge of the absorption band. [c] The indicated energy levels have overlapping transition envelopes and the terms assigned to the energy levels are random and therefore indefinite.

values reported by Carnall.[6] Cursory inspection of Figure 7 shows that some levels, e.g. $^7F_6$, $^5L_6$, and $^7F_4$, are significantly (>100 cm^{-1}) different from those reported by Carnall. This difference may be due to method and equipment, and the comparison within the series are more interesting. Here, the variations are smaller although a clear difference between the four species are seen in $^7F_2$ and $^5G_2$. The differences are not large enough (<100 cm^{-1}) to be assigned to a general change in the electronic energy level, and may simply be due to a redistribution of the many microstates included in the generalised energy level descriptor.

In the absorption spectrum it is difficult to discern the individual microstates, but in emission spectrum the non-degenerate $^5D_0$ state enables the microstates to be resolved in the bands of lower degeneracy. The microstates in $^7F_2$, $^7F_1$ and $^7F_0$ can be assigned with some confidence, and the distribution of microstates $^7F_4$ and $^7F_3$ can be determined. The latter assumes that the transition between the single microstate of $^5D_0$ and each of the microstates in $^7F_4$ and $^7F_3$ are of equal probability. This is a major assumption, as there are no first principle arguments that allows us to predict the transition probability between the microstates. Each microstate is a distinct electronic state, and not a part of a vibronic envelope. In contrast, the distribution of the microstates are well described as it is governed by ligand field theory.[110] In this regard it is interesting to note that the splitting of the three microstates of $^7F_1$ are in a 1:2 group in $[Eu(DPA)(H_2O)_6]^{+}$ (**1**), three resolved microstates in $[Eu(DPA)_2(H_2O)_3]^{-}$ (**2**), and a 1:2 group in

$[Eu(DPA)_3]^{3-}$ (**3**), see Figure 6. Note that the aqua ion, $[Eu(H_2O)_9]^{3+}$ (**0**), is not one distinct species and the ligand field splitting cannot be resolved. This is true for all species when considering $^7F_2$ and $^7F_3$. The nine microstates of $^7F_4$ are not all resolved, but the distribution of the microstates clearly changes between the species. Even though the component spectra are determined, not all microstates are resolved, and we are not able to correlate spectral shape to physical structure.

Conclusions

We have revisited the solution chemistry of the classical europium(III)-dipicolinate system and could show that all the species involved from europium(III) aqua ion, over the mono- and bis-dipicolinates, to the repeatedly investigated europium(III) tris-dipicolinate can be resolved using optical spectroscopy. We conclude that the speciation of these complexes cannot be determined using luminescence spectroscopy, as a weighted average introduce errors as high as 30 %. These results infer that similar errors can be observed for all complexes between smaller ligands and lanthanide(III) ions in aqueous solution.

We were able to resolve the component spectra of each of the species, and from these determine the electronic energy levels and the relative transition probabilities between these. The most crucial finding is that the data show that the probability of $^5D_0 \rightarrow {}^7F_1$ transition is not constant. This result is highly controversial and additional experimental evidence is needed to either support this claim or disprove it. Yet the data presented here indicates that the assumption that the pronounced magnetic dipole nature of this transition leads to a transition probability that is not influenced by the ligand field is wrong.

Based on our findings, we must conclude that some aspects of europium(III) photophysics have yet to be uncovered. The 49 distinct radiative transitions are still to be resolved experimentally and described theoretically.

Conflicts of interest

There are no conflicts to declare

Acknowledgements

The authors thank Carlsbergfondet, Villum Fonden (grants #14922 and #1541), and the University of Copenhagen for support. We furthermore thank DANSCATT (supported by the Danish Agency for Science and Higher Education) for support. Use of the Advanced Photon Source at Argonne National Laboratory was supported by the U. S. Department of Energy, Office of Science, Office of Basic Energy Sciences, under Contract No. DE-AC02-06CH11357.

Notes and references

1. Sharpe, C. H. a. A. *Pearson* **2012,** 4th edition.
2. Carnall, W.; Fields, P.; Rajnak, K. *The Journal of Chemical Physics* **1968,** 49, (10), 4450-4455.
3. Carnall, W.; Fields, P.; Rajnak, K. *The Journal of Chemical Physics* **1968,** 49, (10), 4412-4423.
4. Judd, B. R. *Physical Review* **1962,** 127, (3), 750-&.
5. Reid, M. F.; Richardson, F. *The Journal of Physical Chemistry* **1984,** 88, (16), 3579-3586.
6. Carnall, W. T.; Goodman, G. L.; Rajnak, K.; Rana, R. S. *The Journal of Chemical Physics* **1989,** 90, (7), 3443-3457.
7. Rinehart, J. D.; Long, J. R. *Chemical Science* **2011,** 2, (11), 2078-2085.
8. Caravan, P. *Chemical Society Reviews* **2006,** 35, (6), 512-523.
9. Caravan, P.; Ellison, J. J.; McMurry, T. J.; Lauffer, R. B. *Chemical Reviews* **1999,** 99, (9), 2293-2352.
10. Louie, A. Y.; Hüber, M. M.; Ahrens, E. T.; Rothbächer, U.; Moats, R.; Jacobs, R. E.; Fraser, S. E.; Meade, T. J. *Nature Biotechnology* **2000,** 18, (3), 321-325.
11. Major, J. L.; Meade, T. J. *Accounts of Chemical Research* **2009,** 42, (7), 893-903.
12. Zhang, S.; Merritt, M.; Woessner, D. E.; Lenkinski, R. E.; Sherry, A. D. *Acc Chem Res* **2003,** 36, (10), 783-90.
13. Woods, M.; Woessner, D. E.; Sherry, A. D. *Chemical Society reviews* **2006,** 35, (6), 500-511.
14. Zwier, J. M.; Hildebrandt, N., Time-gated FRET detection for multiplexed biosensing. In *Reviews in Fluorescence 2016*, Springer: 2017; pp 17-43.
15. Sørensen, T. J.; Faulkner, S. *Accounts of chemical research* **2018,** 51, (10), 2493-2501.
16. Montgomery, C. P.; Murray, B. S.; New, E. J.; Pal, R.; Parker, D. *Accounts of chemical research* **2009,** 42, (7), 925-937.
17. Simpson, M.; Kaptur, M.; Alexander, L.; Feinstein, D. **2017,** U.S. Department of Energy - Report to Congress.
18. Moss, R. L.; Tzimas, E.; Willlis, P.; Arendorf, J.; Tercero Espinoza, L.; al., e. **2013,** JRC - Institute for Energy and Transport.
19. Werts, M. H. V. *Science Progress* **2005,** 88, (2), 101-131.
20. Baldo, M.; Thompson, M.; Forrest, S. *Pure and Applied Chemistry* **1999,** 71, (11), 2095-2106.
21. Helm, L.; Merbach, A. E. *Chemical reviews* **2005,** 105, (6), 1923-1960.
22. Horrocks, W. D.; Sudnick, D. R. *Journal of the American Chemical Society* **1979,** 101, (2), 334-340.
23. Chauvin, A. S.; Gumy, F.; Imbert, D.; Bünzli, J. C. G. *Spectroscopy Letters* **2004,** 37, (5), 517-532.
24. Nielsen, L. G.; Sørensen, T. J. *Inorganic Chemistry* **2020**, (59), 94-105.
25. George, M. R.; Golden, C. A.; Grossel, M. C.; Curry, R. J. *Inorganic chemistry* **2006,** 45, (4), 1739-1744.
26. Bünzli, J. C. G.; Pradervand, G. O. *The Journal of Chemical Physics* **1986,** 85, (5), 2489-2497.
27. Binnemans, K.; VanHerck, K.; GorllerWalrand, C. *Chemical Physics Letters* **1997,** 266, (3-4), 297-302.
28. Werts, M. H. V.; Jukes, R. T. F.; Verhoeven, J. W. *Physical Chemistry Chemical Physics* **2002,** 4, (9), 1542-1548.
29. Horrocks, W.; Sudnick, D. *Science* **1979,** 206, (4423), 1194-1196.
30. Guilford Jones, I.; Vullev, V. I. *Photochemical & Photobiological Sciences* **2002,** 1, (12), 925-933.
31. Tancrez, N.; Feuvrie, C.; Ledoux, I.; Zyss, J.; Toupet, L.; Le Bozec, H.; Maury, O. *Journal of the American Chemical Society* **2005,** 127, (39), 13474-13475.

32. D'Aléo, A.; Picot, A.; Beeby, A.; Gareth Williams, J. A.; Le Guennic, B.; Andraud, C.; Maury, O. *Inorganic Chemistry* **2008,** 47, (22), 10258-10268.
33. Eliseeva, S. V.; Auböck, G.; van Mourik, F.; Cannizzo, A.; Song, B.; Deiters, E.; Chauvin, A.-S.; Chergui, M.; Bünzli, J.-C. G. *The Journal of Physical Chemistry B* **2010,** 114, (8), 2932-2937.
34. Grenthe, I. *J. Am. Chem. Soc.* **1961,** 83, (null), 360.
35. Tanner, P. A. *Chemical Society Reviews* **2013,** 42, (12), 5090-5101.
36. Judd, B. R. *The Journal of Chemical Physics* **1979,** 70, (11), 4830-4833.
37. Jean-claude, G. B. *Inorganica Chimica Acta* **1987,** 139, (1-2), 219-222.
38. New, E. J.; Parker, D.; Smith, D. G.; Walton, J. W. *Current Opinion in Chemical Biology* **2010,** 14, (2), 238-246.
39. Faulkner, S.; Pope, S. J. A.; Burton-Pye, B. P. *Applied Spectroscopy Reviews* **2005,** 40, (1), 1-31.
40. Gunnlaugsson, T.; Leonard, J. P. *Chemical Communications* **2005**, (25), 3114-3131.
41. Smith, D. G.; McMahon, B. K.; Pal, R.; Parker, D. *Chemical Communications* **2012,** 48, (68), 8520-8522.
42. Drew, M. G. B. *Coordination Chemistry Reviews* **1977,** 24, (2), 179-275.
43. Nielsen, L. G.; Junker, A. K. R.; Sorensen, T. J. *Dalton Transactions* **2018**.
44. Persson, I.; D'Angelo, P.; De Panfilis, S.; Sandström, M.; Eriksson, L. *Chemistry – A European Journal* **2008,** 14, (10), 3056-3066.
45. Thomson, J. J. *The London, Edinburgh, and Dublin Philosophical Magazine and Journal of Science* **1904,** 7, (39), 237-265.
46. Albertsson, J. *Acta Chem. Scand* **1972,** 26, (3), 1023-1044.
47. Rajnak, K.; Couture, L. *Chemical Physics* **1981,** 55, (3), 331-337.
48. Bünzli, J. C. G.; Chauvin, A. S. *Spectroscopy Letters* **2004,** 37, (5), 517-532.
49. D'Aléo, A.; Toupet, L.; Rigaut, S.; Andraud, C.; Maury, O. *Optical Materials* **2008,** 30, (11), 1682-1688.
50. Heathman, C. R.; Nash, K. L. *Separation Science and Technology* **2012,** 47, (14-15), 2029-2037.
51. Sharma, G.; Narula, A. K. *Journal of Materials Science: Materials in Electronics* **2015,** 26, (2), 1009-1017.
52. Moore, E. G. *Dalton Transactions* **2012,** 41, (17), 5272-5279.
53. Picot, A.; D'Aléo, A.; Baldeck, P. L.; Grichine, A.; Duperray, A.; Andraud, C.; Maury, O. *Journal of the American Chemical Society* **2008,** 130, (5), 1532-1533.
54. Andres, J.; Borbas, K. E. *Inorganic chemistry* **2015,** 54, (17), 8174-8176.
55. Gassner, A.-L.; Duhot, C.; G. Bünzli, J.-C.; Chauvin, A.-S. *Inorganic chemistry* **2008,** 47, (17), 7802-7812.
56. Adumeau, P.; Gaillard, C.; Boyer, D.; Canet, J. L.; Gautier, A.; Mahiou, R. *European Journal of Inorganic Chemistry* **2015,** 2015, (7), 1233-1242.
57. Gaillard, C.; Adumeau, P.; Canet, J.-L.; Gautier, A.; Boyer, D.; Beaudoin, C.; Hesling, C.; Morel, L.; Mahiou, R. *Journal of Materials Chemistry B* **2013,** 1, (34), 4306-4312.
58. Kaczmarek, A. M. *Journal of Materials Chemistry C* **2018,** 6, (22), 5916-5925.
59. Kumar, D.; Tewari, S.; Adnan, M.; Ahmad, S.; Prakash, G. V.; Ramanan, A. *Inorganica Chimica Acta* **2019,** 487, 81-91.
60. Liu, H. X.; Liu, Q.; Xu, Y.; Huang, T. T.; Wang, L. T.; Ye, K. Q.; Zeng, G. In *Study on a Structure of 2, 6-Pyridine-Dicarboxylic Acid Europium Quarthydrate*, Advanced Materials Research, 2014; Trans Tech Publ: pp 490-493.
61. Niu, Z.; Fang, S.; Ma, J.-G.; Zhang, X.-P.; Cheng, P. *Chemical Communications* **2014,** 50, (58), 7797-7799.
62. Park, H.-J.; Ko, S.-B.; Wyman, I. W.; Wang, S. *Inorganic chemistry* **2014,** 53, (18), 9751-9760.
63. Tao, C.; Du, K.; Yin, Q.; Zhu, J.; Yan, H.; Zhu, F.; Zhang, L. *RSC Advances* **2015,** 5, (72), 58936-58942.
64. Wang, N.; Wang, J.; Zhao, D.; Mellerup, S. K.; Peng, T.; Wang, H.; Wang, S. *Inorganic chemistry* **2018,** 57, (16), 10040-10049.
65. Xu, L.; Jing, Y.; Feng, L.; Xian, Z.; Yan, Y.; Liu, Z.; Huang, J. *Physical Chemistry Chemical Physics* **2013,** 15, (39), 16641-16647.
66. Binnemans, K. *Coordination Chemistry Reviews* **2015,** 295, 1-45.
67. Horrocks, W. D.; Arkle, V. K.; Liotta, F. J.; Sudnick, D. R. *Journal of the American Chemical Society* **1983,** 105, (11), 3455-3459.
68. Nielsen, L. G.; Sørensen, T. J. *Inorganic Chemistry* **2019**.
69. Supkowski, R. M.; Horrocks, W. D. *Inorganica Chimica Acta* **2002,** 340, 44-48.
70. Haas, Y.; Stein, G. *The Journal of Physical Chemistry* **1971,** 75, (24), 3668-3677.
71. Powell, D. H.; Merbach, A. E. *Magnetic Resonance in Chemistry* **1994,** 32, (12), 739-745.
72. Strickler, S. J.; Berg, R. A. *The Journal of chemical physics* **1962,** 37, (4), 814-822.
73. Beeby, A.; Clarkson, I. M.; Dickins, R. S.; Faulkner, S.; Parker, D.; Royle, L.; de Sousa, A. S.; Williams, J. A. G.; Woods, M. *Journal of the Chemical Society, Perkin Transactions 2* **1999**, (3), 493-504.
74. Tropiano, M.; Blackburn, O. A.; Tilney, J. A.; Hill, L. R.; Just Sørensen, T.; Faulkner, S. *Journal of Luminescence* **2015,** 167, 296-304.
75. I, T.-P.; Nancollas, G. H. *Analytical chemistry* **1972,** 44, (12), 1940-1950.
76. Kuzmič, P. *Analytical Biochemistry* **1996,** 237, (2), 260-273.
77. Kuzmič, P., Chapter 10 - DynaFit—A Software Package for Enzymology. In *Methods in Enzymology*, Johnson, M. L.; Brand, L., Eds. Academic Press: 2009; Vol. 467, pp 247-280.
78. John E. Dennis, J.; Gay, D. M.; Welsch, R. E. *ACM Trans. Math. Softw.* **1981,** 7, (3), 369-383.
79. Bates, D. M.; Watts, D. G., *Nonlinear Regression Analysis and its Applications*. Wiley, New York, 1988.
80. Hammersley, A. *European Synchrotron Radiation Facility Internal Report ESRF97HA02T* **1997,** 68, 58.
81. Juhas, P.; Davis, T.; Farrow, C. L.; Billinge, S. J. L. *Journal of Applied Crystallography* **2013,** 46, (2), 560-566.
82. Ofelt, G. S. *Journal of Chemical Physics* **1962,** 37, (3), 511-&.
83. Görller-Walrand, C.; Fluyt, L.; Ceulemans, A.; Carnall, W. T. *The Journal of Chemical Physics* **1991,** 95, (5), 3099-3106.
84. Kofod, N.; Arppe-Tabbara, R.; Sørensen, T. J. *The Journal of Physical Chemistry A* **2019,** 123, (13), 2734-2744.
85. Blackburn, O. A.; Tropiano, M.; Sørensen, T. J.; Thom, J.; Beeby, A.; Bushby, L. M.; Parker, D.; Natrajan, L. S.; Faulkner, S. *Physical Chemistry Chemical Physics* **2012,** 14, (38), 13378-13384.
86. Atkins, P. W.; De Paula, J.; Friedman, R. S.; Oxford University, P., *Physical chemistry : quanta, matter, and change*. Oxford University Press: Oxford, 2014.
87. Johansson, G.; Magini, M.; Ohtaki, H. *Journal of Solution Chemistry* **1991,** 20, (8), 775-792.
88. Neuefeind, J.; Skanthakumar, S.; Soderholm, L. *Inorganic Chemistry* **2004,** 43, (7), 2422-2426.
89. Soderholm, L.; Skanthakumar, S.; Neuefeind, J. *Analytical and Bioanalytical Chemistry* **2005,** 383, (1), 48-55.
90. Bünzli, J.-C.; Eliseeva, S., Basics of Lanthanide Photophysics. 2010; Vol. 7, pp 1-45.
91. Tanner, P. A. *Springer Ser. Fluoresc.* **2011,** 7, 183-234.
92. Binnemans, K.; Görller-Walrand, C. *Chemical Physics Letters* **1995,** 245, (1), 75-78.

93. Parker, D. *Chemical Society Reviews* **2004,** 33, (3), 156-165.
94. Mason, K.; Harnden, A. C.; Patrick, C. W.; Poh, A. W. J.; Batsanov, A. S.; Suturina, E. A.; Vonci, M.; McInnes, E. J. L.; Chilton, N. F.; Parker, D. *Chemical Communications* **2018,** 54, (61), 8486-8489.
95. Albin, M.; Farber, G. K.; Horrocks, W. D. *Inorganic Chemistry* **1984,** 23, (12), 1648-1651.
96. Karraker, D. G. *Journal of Chemical Education* **1970,** 47, (6), 424.
97. Stephens, E. M.; Davis, S.; Reid, M. F.; Richardson, F. *Inorganic Chemistry* **1984,** 23, (26), 4607-4611.
98. D'Aléo, A.; Picot, A.; Baldeck, P. L.; Andraud, C.; Maury, O. *Inorganic Chemistry* **2008,** 47, (22), 10269-10279.
99. Aebischer, A.; Gumy, F.; Bünzli, J.-C. G. *Physical Chemistry Chemical Physics* **2009,** 11, (9), 1346-1353.
100. Tanner, P. A.; Zhou, L.; Duan, C.; Wong, K.-L. *Chemical Society Reviews* **2018,** 47, (14), 5234-5265.
101. Turro, N. J., *Modern Molecular Photochemistry* University Science Books Sausalito, 1991; p 628.
102. Kasha, M. *Acta Phys. Pol. A* **1999**, 15-36.
103. Riehl, J. P.; Richardson, F. S. *Chem. Rev.* **1986,** 86, (1), 1-16.
104. Richardson, F. S. *Inorganic chemistry* **1980,** 19, (9), 2806-2812.
105. Turro, N. J., *Modern molecular photochemistry*. University science books: 1991.
106. Strickler, S. J.; Berg, R. A. *J. Chem. Phys.* **1962,** 37, (4), 814-&.
107. Hirayama, S.; Phillips, D. *Journal of Photochemistry* **1980,** 12, (2), 139-145.
108. Kasha, M. *Acta Phys. Polon. A* **1999,** 95, 15-36.
109. Lewis, G. N.; Kasha, M. *Journal of the American Chemical Society* **1945,** 67, (6), 994-1003.
110. Figgis, B. N., *Ligand field theory and its applications / Brian N. Figgis, Michael A. Hitchman*. Wiley-VCH: New York, 2000.